AGU PUBLICATIONS

Journal of Advances in Modeling Earth Systems

RESEARCH ARTICLE
10.1002/2015MS000495

Special Section:
The 2011–12 Indian Ocean Field Campaign: Atmospheric-Oceanic Processes and MJO Initiation

Initiation of an intraseasonal oscillation in an aquaplanet general circulation model

Eric D. Maloney[1] and Brandon O. Wolding[1]

[1]Department of Atmospheric Science, Colorado State University, Fort Collins, Colorado, USA

Abstract MJO initiation is studied in an aquaplanet general circulation model that has strong and highly regular MJO-like variability. About 80% of MJO events in the model are found to be successive events, immediately preceded by another strong MJO event. Hence, the dynamics of MJO initiation in the model are dominated by interactions with preceding events. Rossby gyres associated with the previous cycle of suppressed MJO convection to the east are shown to help initiate the next cycle of MJO convection in the western warm pool, consistent with the recent study of Zhao et al. (2013). Meridional and vertical moisture advection associated with the anomalous Rossby gyres help to moisten the MJO initiation region in advance of convective onset. An experiment is conducted in which circumnavigating Kelvin waves and their influence on the MJO initiation region are suppressed. While MJO activity in the model is just as regular with suppression of circumnavigation, MJO amplitude is reduced relative to the control simulation, especially in the western part of the warm pool. Possible physical mechanisms responsible for this change in MJO amplitude are discussed, including the role of low-level moisture convergence anomalies induced by circumnavigating Kelvin waves, and interactions with mean state changes.

Key Points:
- MJO initiation is diagnosed in an aquaplanet model with highly regular MJO
- Rossby gyres help initiate the next cycle of MJO convection
- Circumnavigating Kelvin waves modulate the amplitude but not regularity of events

Correspondence to:
E. D. Maloney,
emaloney@atmos.colostate.edu

Citation:
Maloney, E. D., and B. O. Wolding (2015), Initiation of an intraseasonal oscillation in an aquaplanet general circulation model, *J. Adv. Model. Earth Syst.*, *7*, 1956–1976, doi:10.1002/2015MS000495.

Received 9 JUN 2015
Accepted 14 SEP 2015
Accepted article online 18 SEP 2015
Published online 9 DEC 2015

1. Introduction

Understanding the initiation of the Madden-Julian oscillation (MJO) is a topic that has received increasing attention during the last decade. Basic questions still remain about the dynamics of MJO initiation, including how frequently MJO events are preceded and initiated by a previous MJO event. *Matthews* [2008] defines two types of MJO events, primary and successive, with the latter defined as being preceded by an existing MJO event. Using an observational data set, *Matthews* [2008] classified 60% of MJO events as successive. *Matthews* [2008] showed that successive events appear to be preceded by Kelvin wave circumnavigation, frictional moisture convergence, and warm Indian Ocean SST anomalies, although formation processes may be different for primary events. However, *Straub* [2013] noted that both primary and successive events tend to be associated with similar precursor dynamical signatures, making the distinction between the two difficult to clearly define. We will set aside the distinction between primary and successive events for now, and simply discuss some of the mechanisms that have been recently proposed for MJO initiation. While previous studies have found that MJO convective initiation does not occur exclusively in the Indian Ocean [e.g., *Straub*, 2013], the following discussion of initiation will focus on the Indian Ocean.

Extratropical initiation mechanisms for the MJO have been a focus of past research. *Hsu et al.* [1990] documented the possible influence of an extratropical Rossby wave train on development of MJO convection in the Indian Ocean during the boreal winter of 1985–1986. *Bladé and Hartmann* [1993] argued for an important role for midlatitude baroclinic eddies in triggering Indian Ocean MJO convection. This hypothesis was supported by *Wang et al.* [2012], who argued that an Asian cold surge helped initiate MJO convection in the western Indian Ocean in January of 2008. *Pan and Li* [2008] used a 2.5 layer model to investigate the role of southeastward propagating Rossby wave packets from midlatitudes in initiating Indian Ocean convection. *Ray et al.* [2009] used a tropical channel model to demonstrate an influence of extratropical forcing on MJO initiation, with a later study showing that eddy momentum flux convergence helps to initiate MJO events in this model through the forcing of the Indian Ocean zonal flow [*Ray and Zhang*, 2010]. *Ray and Li* [2013] showed in a GCM that removing extratropical influences weakened MJO events in the Indian Ocean, mainly through their effect on the mean state. We will not address the role of extratropical initiation processes in this study. The model experiments we conduct will be characterized by weakened meridional SST gradients

and hence weakened midlatitude eddy activity and midlatitude jets. However, we cannot rule out that important tropical-extratropical interactions, such as projection of the extratropics onto the tropics [e.g., *Hoskins and Yang*, 2000], can occur in our model given that its MJO initiation region is off the equator.

Another proposed mechanism for initiation of Indian Ocean MJO activity is equatorial Kelvin wave circumnavigation associated with the previous cycle of suppressed MJO convection over the west Pacific. *Kikuchi and Takayabu* [2003] argued that frictional moisture convergence forced by dry Kelvin wave propagation from the MJO in the west Pacific through the Western Hemisphere helps to initiate the next round of Indian Ocean MJO convection. *Matthews* [2008] argues that cold temperature anomalies associated with circumnavigating Kelvin waves modulate Indian Ocean static stability and can foster the next cycle of MJO convection. *Powell and Houze* [2015] argue for an important role for circumnavigating equatorial signals and associated upper tropospheric vertical velocity signals to the initiation of Indian Ocean MJO events in the boreal fall of 2011. Previous MJO composite studies exhibited dynamical structures consistent with the behavior suggested above [e.g., *Hendon and Salby*, 1994; *Knutson and Weickmann*, 1987]. Modeling studies provide mixed findings on the importance of Kelvin wave circumnavigation to MJO initiation. In a Lagrangian aquaplanet global atmosphere model, *Haertel et al*. [2014] describe a potentially important role for circumnavigating Kelvin waves forced by preceding MJO events for initiating the next cycle of suppressed or enhanced convection. Convection was primarily modulated by the deep temperature perturbations associated with the forced Kelvin waves, consistent with a mechanism proposed by *Matthews* [2008], and also supported by the composites of *Straub* [2013]. However, in a GCM with realistic continental distributions, *Ray and Li* [2013] suppressed circumnavigating Kelvin waves by relaxing model prognostic variables in the tropical Atlantic to their climatology, and found an insignificant impact on the simulated MJO. Similarly, *Zhao et al*. [2013] used a general circulation model with an Atlantic damping zone to demonstrate that Kelvin wave circumnavigation is not critical for Indian Ocean MJO initiation in their model. We will contribute to this debate and test the potential importance of Kelvin wave circumnavigation to the simulated MJO in an aquaplanet GCM, using a method similar to that of *Ray and Li* [2013] to damp Kelvin wave circumnavigation.

Other studies have proposed regional and local mechanisms for initiation and forcing of Indian Ocean MJO events, including forcing by the previous cycle of MJO convection. For example, *Wang and Xie* [1997] hypothesized that westward Rossby wave propagation from the previous cycle of enhanced convection in the west Pacific can reinitiate intraseasonal convection in the western Indian Ocean, particularly during boreal summer. *Webber et al*. [2010, 2012] argued that oceanic Rossby waves forced by MJO events and their induced SST anomalies in the Indian Ocean can help initiate MJO events. *DeMott et al*. [2014] discuss the general role that Indian Ocean SST anomalies and associated flux anomalies may play in growing MJO convective events in the Indian Ocean. The role of horizontal advective moistening in the Indian Ocean for priming the troposphere for subsequent MJO deep convection has also received considerable recent attention. *Kiranmayi and Maloney* [2011a] demonstrated using reanalysis data that anomalous zonal moisture advection, primarily through anomalous zonal winds acting on the mean Indian Ocean moisture gradient, helps to moisten the atmosphere in advance of subsequent MJO convection. In a more comprehensive analysis, *Zhao et al*. [2013] showed that anomalous Rossby wave circulations forced by the previous cycle of suppressed MJO convection can moisten the MJO initiation region through anomalous zonal and meridional moisture advection, primarily through advection by the anomalous flow across the mean moisture gradient.

Interest in Indian Ocean MJO initiation has also accelerated recently in association with the Cooperative Indian Ocean Experiment on Intraseasonal Variability in the Year 2011 (CINDY2011)/Dynamics of the MJO (DYNAMO)/ARM MJO Investigation Experiment (AMIE) field campaign conducted in the equatorial Indian Ocean for boreal Fall 2011 through boreal winter 2012 [*Yoneyama et al*., 2013]. The large-scale conditions associated with DYNAMO period MJO events, and interactions with other time scale variability, are discussed in *Gottschalck et al*. [2013]. While analysis of observations and supporting modeling studies from this field experiment is still in their early phase, important insight has already been gained on MJO initiation. In particular, much work has been conducted to understand tropospheric moistening processes that precede MJO convective initiation in the Indian Ocean, and subsequent moisture evolution.

Johnson and Ciesielski [2013] documented basic MJO behavior from the DYNAMO sounding arrays, including the evolution of the vertical moisture structure during MJO events. *Sobel et al*. [2014] showed that both

horizontal and vertical moisture advection played important roles in moistening the atmosphere prior to the initiation of the DYNAMO MJO events and also argued that radiative feedbacks help to destabilize the MJO. The cloud resolving model of *Wang et al*. [2015] produced results broadly consistent with the observational analysis of *Sobel et al*. [2014], although the model was characterized by stronger wind-evaporation feedbacks and weaker radiative feedbacks than observed. Using thermodynamic and moisture budgets derived from the DYNAMO sounding arrays, *Johnson et al*. [2015] documented the evolution of convective systems, as well as their contributions to tropospheric moistening. This study also highlighted an important role for radiative feedbacks for destabilizing the MJO in the initiation region, consistent with the findings of *Sobel et al*. [2014]. *Nasuno et al*. [2015] used ECMWF reanalysis fields to show that horizontal advection in regions of anomalous intraseasonal easterly flow was an important moistening mechanism in advance of DYNAMO MJO convective events, consistent with previous work [e.g., *Maloney*, 2009; *Sobel et al*., 2014; *Kiranmayi and Maloney*, 2011a; *Zhao et al*., 2013]. *Kerns and Chen* [2014] highlighted a potentially important role for dry intrusions from the subtropics in initiation MJO convection by suppressing convection in the ITCZ region and fostering subsequent equatorial ascent that moistens and supports equatorial convection. This study also examined the role of dry advection associated with synoptic gyres in the MJO convective envelope for terminating MJO convection and contributing to eastward propagation.

DYNAMO observations have also been used to assess the recharge-discharge hypothesis for MJO dynamics [e.g., *Benedict and Randall*, 2007]. *Powell and Houze* [2013] documented the rapid humidification of the free troposphere in advance of MJO events in the DYNAMO period and argued that the moistening rate was faster than that suggested by the "recharge-discharge" paradigm for the MJO in which shallow convective moistening helps to set the MJO time scale. However, using radar fields from the *R/V Roger Revelle*, *Xu and Rutledge* [2014] argued that the evolution of DYNAMO cloud populations and tropospheric moisture supported the recharge-discharge paradigm. Similarly, *Bellenger et al*. [2015] quantified tropospheric moistening processes using data from the *R/V Mirai* during DYNAMO and found a significant role for shallow convection in moistening the atmosphere in advance of deeper convection.

Other studies have examined surface energy budget and SST variations during the DYNAMO period and their role in maintaining tropospheric moisture anomalies that support MJO convection. *De Szoeke et al*. [2015] diagnosed the surface energy budget and SST variations during DYNAMO MJO events and quantified the importance of surface evaporation anomalies in maintaining MJO convection. The analysis also suggested a possible role for SST-induced moisture convergence in supporting moistening associated with the MJO, although further research is needed to quantify this link. However, *Fu et al*. [2015] used observations and model hindcasts of DYNAMO MJO events to show that the importance of SST anomalies to MJO dynamics varied strongly from event to event.

The evidence discussed above suggests that understanding the processes that drive tropospheric moistening may be important to understanding MJO initiation. In this context, a growing body of research over the last several years has viewed the MJO from the paradigm of a moisture mode, a disturbance that exists under conditions of weak tropical temperature gradients, and whose destabilization and propagation mechanisms are regulated by the processes controlling the tropospheric moisture budget [e.g., *Raymond and Fuchs*, 2009; *Sobel and Maloney*, 2012, 2013]. Under this paradigm, previous work has suggested the importance of horizontal moisture advection for regulating eastward propagation of the MJO [*Maloney*, 2009; *Andersen and Kuang*, 2012; *Pritchard and Bretherton*, 2014; *Chikira*, 2014], and radiative and wind-evaporation feedbacks for destabilizing the MJO [e.g., *Raymond*, 2001; *Maloney and Sobel*, 2004; *Andersen and Kuang*, 2012; *Chikira*, 2014; *Wolding and Maloney*, 2015].

This paper will examine moistening processes associated with MJO initiation in a modified version of the NCAR Community Atmosphere Model version 3.1 (CAM3), run in aquaplanet mode. Previous studies have shown that this model configuration produces extremely strong and regular MJO-like variability [*Maloney et al*., 2010; *Kiranmayi and Maloney*, 2011b; *Maloney and Xie*, 2013]. We will specifically examine the composite moisture budget of the model in the context of MJO initiation, with the aim of identifying salient processes that regulate the initiation of the MJO in the real world, with primary relevance to successive events. The role of Kelvin wave circumnavigation is a particular focus of this study, and we will conduct sensitivity experiments to remove the influence of circumnavigating Kelvin waves to assess their role in initiating successive events and producing the strong regularity of MJO activity in the model.

The aquaplanet modeling framework used here is highly idealized, and the real Earth admittedly adds more complications to the MJO initiation process. However, many features of the MJO initiation process in the aquaplanet model that we will describe, including Kelvin wave circumnavigation and influence from Rossby gyres forced by the previous cycle of MJO convection have also been documented in the real world [e.g., *Matthews*, 2008; *Zhao et al*., 2013]. Therefore, while the dynamics of the aquaplanet model MJO initiation process may contain fewer confounding factors than in reality and represent a purer dynamics, scrutinizing the model behavior will still provide insight into actual MJO initiation. We also note that many general circulation models with realistic land surfaces, including versions of the model used here [e.g., *Maloney*, 2009], exhibit significant MJO simulation deficiencies such as Indian Ocean variability that is weaker than observed. Since our aquaplanet experiment contains a realistic amplitude MJO, it can be argued that examination of the initiation process in the aquaplanet model provides as much or more insight into the MJO initiation process than a flawed model with realistic land distribution.

Section 2 briefly describes the model setup, and presents global characteristics of a model MJO lifecycle, with an emphasis on processes relevant to the moisture budget. Section 3 focuses on moistening processes specific to the MJO initiation region, with the respective roles of horizontal advection and vertical advection examined. Section 4 describes the results of sensitivity tests used to isolate the role of Kelvin wave circumnavigation for initiating successive MJO events. Section 5 presents discussion and conclusions.

2. Model Description and Basic MJO Behavior

2.1. Brief Model Description

As in *Maloney et al*. [2010], we employ a version of the National Center for Atmospheric Research (NCAR) Community Atmosphere Model version 3.1 (CAM3) with the *Zhang and McFarlane* [1995] deep convection parameterization replaced by the relaxed Arakawa-Schubert scheme of *Moorthi and Suarez* [1992]. This implementation includes a minimum convective entrainment threshold as developed by *Tokioka et al*. [1988]. The control simulation we employ is identical to that of *Maloney et al*. [2010], using the perpetual aquaplanet SST boundary condition as shown in Figure 1a. As discussed in more detail in *Maloney et al*. [2010], this SST boundary condition is derived from observations, although has a meridional SST gradient poleward of 10° reduced to one-quarter of that observed. As also discussed in section 1, extratropical synoptic activity is strongly reduced relative to observations given the reduced SST gradient. While this weak extratropical variability may be one reason for the strong regularity of the MJO signal in the model that is discussed in more detail below, it does not entirely exclude an important role for tropical-extratropical interactions in model MJO initiation [e.g., *Hoskins and Yang*, 2000]. The model is run using perpetual 21 March insolation and ozone concentrations for a period of 16 years, with a dynamical core of T42 horizontal resolution and 26 vertical levels.

2.2. Basic Model Behavior

Figure 1b shows a Hovmoller diagram of vertically integrated humidity averaged from 0°S to 20°S for one 200 day segment of the simulation. Even without filtering, the strong regularity of MJO-like activity in the model is apparent, featuring eastward-propagating periods of high precipitable water alternating with dry periods over a cycle of about 40–50 days. Eastward propagation at about 5 m s^{-1} is found across the warm pool, with termination of the propagating humidity features to the east of the Dateline. Strong convective anomalies of amplitude about 12 mm d^{-1} accompany these propagating moisture signals (not shown) [see *Maloney et al*., 2010].

Maloney et al. [2010, Figure 6] showed the two leading spatial structures from a combined empirical orthogonal function (CEOF) analysis of equatorial averaged 20–100 day band pass filtered 850 and 200 hPa zonal wind and outgoing longwave radiation. The leading CEOFs resemble similar CEOFs derived from observations [*Wheeler and Hendon*, 2004], and in combination explain 48% of the total variance. A phase diagram of the leading principal components for a selected 150 day segment of the simulation demonstrates the strong regularity of the intraseasonal oscillation in the model (Figure 2), consistent with the regular variability shown in Figure 1b. Before proceeding, it is useful to quantify the regularity of events in the model. As will be described below, composite positive precipitation anomalies first appear in the western warm pool in Phase 3. The first appearance of the index in Phase 3 with amplitude greater than one is considered to be the initiation of an event, of which we find 82 events over the 16 year simulation. While events in the

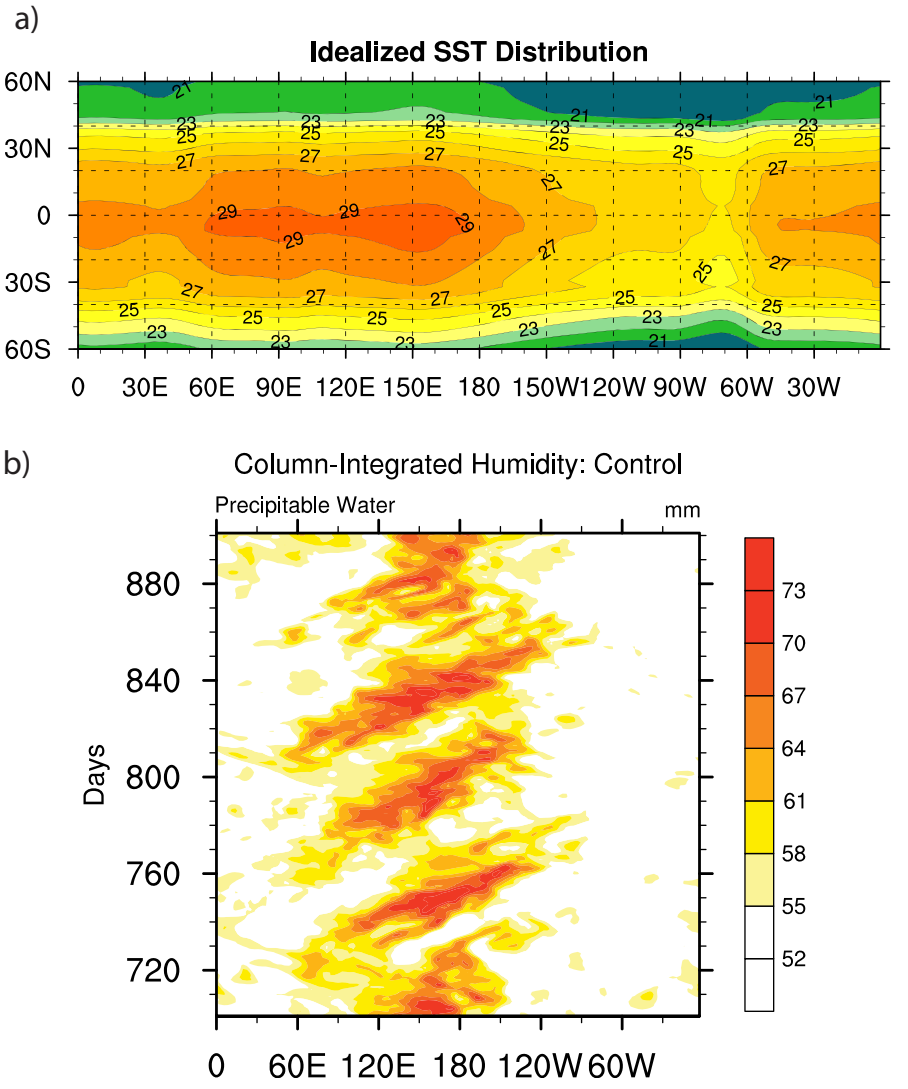

Figure 1. (a) Idealized SST distribution used for the experiments and (b) time-longitude diagram of 0°S–20°S averaged precipitable water for Days 700–900 of the control simulation.

model can begin (i.e., first reach amplitude one) in other phases, here we will concentrate only on events beginning in the western warm pool, since this is the area of interest for the purposes of this study, consistent with the emphasis on the DYNAMO region in recent studies and the location of MJO convective initiation in the canonical MJO. Of these 82 model initiation events, 79% are preceded by a Phase 8 period of amplitude greater than one within the previous 25 days (and also intervening Phases 1 and 2), which suggests that strong precursor events accompany the vast majority of the western warm pool initiations we find here. This statistic is consistent with the regularity seen in Figures 1 and 2. If no amplitude threshold is applied to precursor activity, to include events that *Straub* [2013] considers "intensification" events, 98% of initiation events are preceded by the index cycling through Phases 8, 1, and 2 immediately before onset in Phase 3.

Composite MJO events are now created by averaging together all days that exceed an amplitude of one within each individual phase. Composite 20–100 day bandpass filtered precipitable water (colors) and precipitation (contours) anomalies for Phases 1–8 are shown in Figure 3. Positive precipitation anomalies above 2 mm d^{-1} are first detected in the western part of the warm pool during Phase 3, centered to the south of the equator consistent with the weighting of the mean SST distribution south of the equator (Figure 1a). At later phases this precipitation anomaly intensifies and propagates eastward, eventually decaying to the east of the dateline. Suppressed precipitation anomalies initially appear on the west side of the warm pool during Phase 7, and are

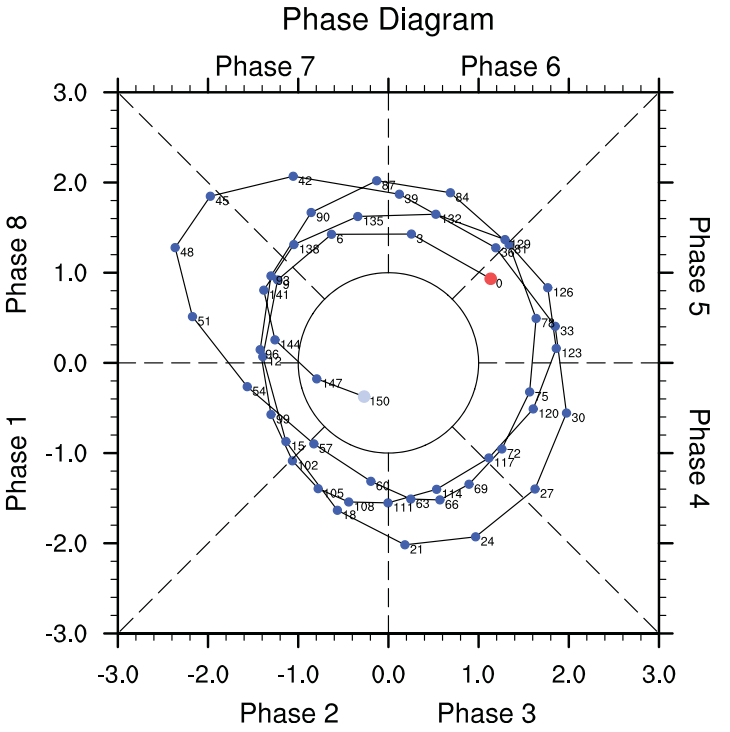

Figure 2. Phase diagram derived from PC1 and PC2 showing the evolution of a 150 day period of the simulation. The unit circle represents an amplitude of one standard deviation. Every third day is plotted with a marker.

similarly located centered south of the equator. In contrast, precipitable water anomalies grow both to the north and south of the equator near 10°N and 10°S during and in advance of the appearance of the Southern Hemisphere precipitation anomaly, a signal that will be discussed in more detail below. Interestingly, precipitation anomalies only form in association with the southern humidity anomaly. Another notable signal in Figure 3 is a tongue of equatorial humidity anomalies that extends eastward from the eastern edge of the warm pool (∼150°W) and circumnavigates the equator at certain phases. This signal is especially apparent in Phases 1 and 5, where a tongue of equatorial moisture penetrates into the west side of the warm pool and precedes the subsequent appearance of precipitation anomalies, although is not collocated with where precipitation anomalies are generated to the south of the equator. This signal is consistent with the circumnavigation of a Kelvin wave forced by a previous cycle of MJO convection [e.g., *Matthews*, 2008; *Haertel et al*., 2014], a hypothesis that will now be examined in more detail.

Composite surface convergence and precipitation anomalies are displayed in Figure 4. Narrow equatorial convergence anomalies during Phases 8 and 1, consistent with convergence into an equatorial Kelvin wave pressure trough forced by MJO heating [e.g., *Maloney and Hartmann*, 1998], precede and coincide with positive equatorial moisture anomalies (Figure 3). Comparable magnitude divergence anomalies during Phases 4 and 5 are associated with development of an equatorial dry tongue. An analysis of vertically integrated moisture convergence minus precipitation anomalies for Phases 8 and 4, the phases that precede the strongest tongue-like equatorial moisture anomaly features in Figure 3, indicates moistening on the equator consistent with equatorial convergence anomalies during Phase 8, and drying due to equatorial divergence during Phase 4 (not shown here). Circumnavigating convergence anomaly fields in the upper troposphere are much less coherent than those at the surface (not shown here).

Figure 4 also indicates notable surface convergence anomalies south of the equator that are out of phase with the equatorial features, also consistent with generation by boundary layer friction. These off-equatorial features may act to reinforce the developing precipitation anomalies near and to the east of the initiation region in Phases 1 and 5. Figure 4 (e.g., Phases 2–4) also suggests that model MJO convection anomalies to the east of the Dateline do not directly force circumnavigating Kelvin wave features given the off-equatorial nature of convection in our model, unlike in *Haertel et al*. [2014] where Kelvin wave forcing by equatorial convection is more direct. Rather, such signals appear to be forced by equatorial dynamical forcing that appears coupled to that in the off-equatorial convective regions, although is of opposite sign. Examination of upper tropospheric wind and stream function anomalies from the control simulation (not shown) also indicates that equatorial easterlies develop near and to the east of 140°W during Phase 3 before rapidly expanding eastward into the warm pool during Phase 4 when convection anomalies are intensifying, as in the observed composites of *Roundy* [2014]. However, unlike in *Roundy* [2014] no strong connection to the

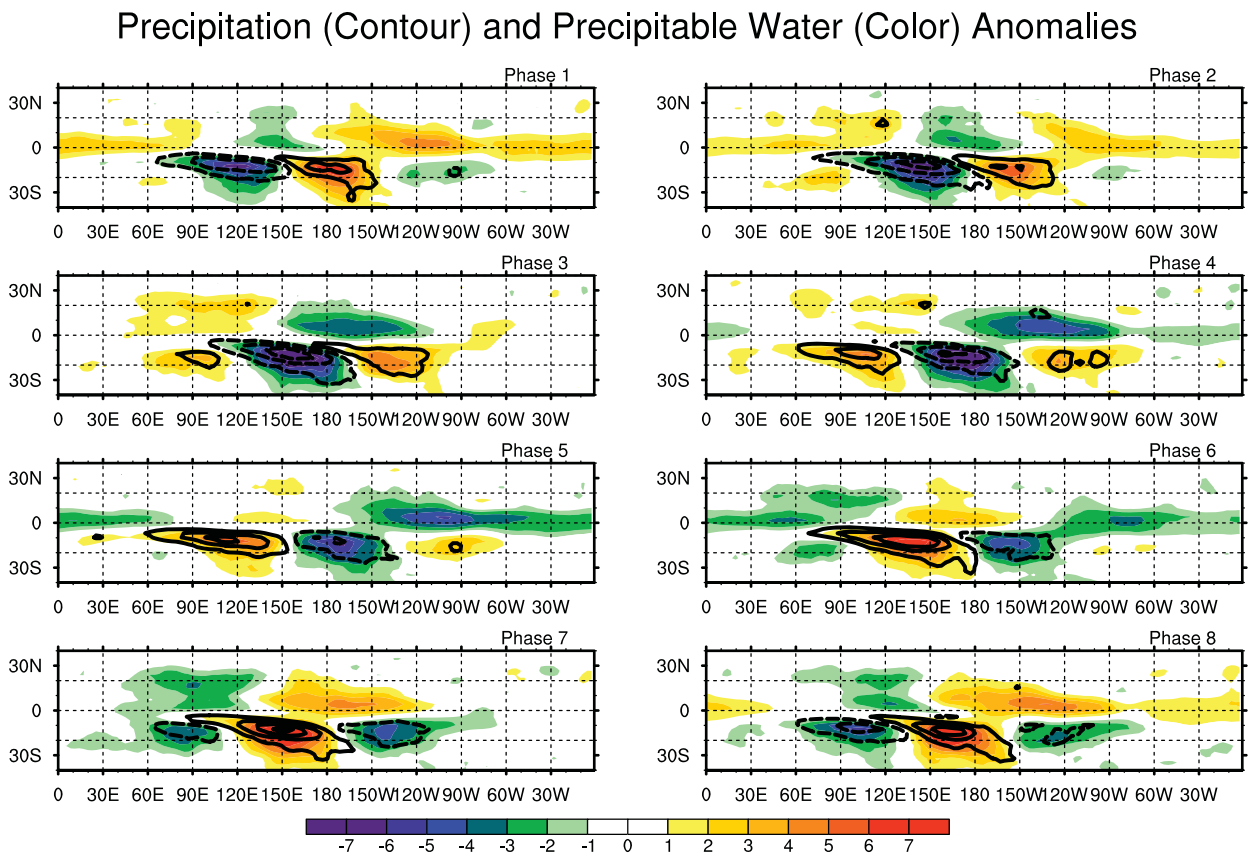

Figure 3. Composite precipitable water (color) and precipitation (contours) anomalies as a function of phase. The precipitable water anomalies have unit of mm. The precipitation anomaly contour interval is 4 mm d^{-1}, starting at 2 mm d^{-1}. Negative contours are dashed.

extratropics associated with this signal is found, although tropical-extratropical interactions will be scrutinized more closely in future work. We also note that circumnavigation appears just as prominently in the *Maloney et al*. [2010] aquaplanet experiment with realistic meridional SST gradient (not shown here), and so further scrutiny of that simulation in the context of tropical-extratropical interactions may prove especially fruitful.

The vertical structure of the meridional convergence field supports the hypothesis that Kelvin wave circumnavigation and associated frictional boundary layer convergence support the narrow equatorial moisture features shown in Figure 3. Figure 5 shows a vertical cross section of Phase 5 meridional wind, omega, and convergence anomalies at 31°E, and extending from 20°S to 20°N. We diagnose Kelvin wave dynamical structure at 31°E because it is a longitude that is to the west of the MJO initiation region, relatively unaffected by the convective processes in the initiation region, and hence relatively pure from a dry dynamical. However, 31°E is also close enough to the initiation region such that dynamical signals diagnosed there will soon after have a downstream impact on MJO initiation. Consistent with boundary layer divergence away from an equatorial pressure ridge associated with a forced dry Kelvin wave (also supported by examination of the temperature structure, not shown), meridional flow anomalies diverge in the boundary layer below 900 mb, and converge (more weakly) just above this level. The omega anomalies are characteristic of a relatively shallow circulation in this region and others away from the warm pool, with little apparent connection to the middle and upper troposphere. This shallow return flow solution is consistent with that expected from near-equatorial forced upward motion at the boundary layer top in the absence of substantial interaction with diabatic heating [e.g., *Gonzalez and Mora Rojas*, 2014]. Consistent with Figure 4, boundary layer convergence anomalies occur near 10°S, which will be shown in section 4 to be potentially important for supporting the off-equatorial convection anomaly in the MJO initiation region (e.g., Figure 3).

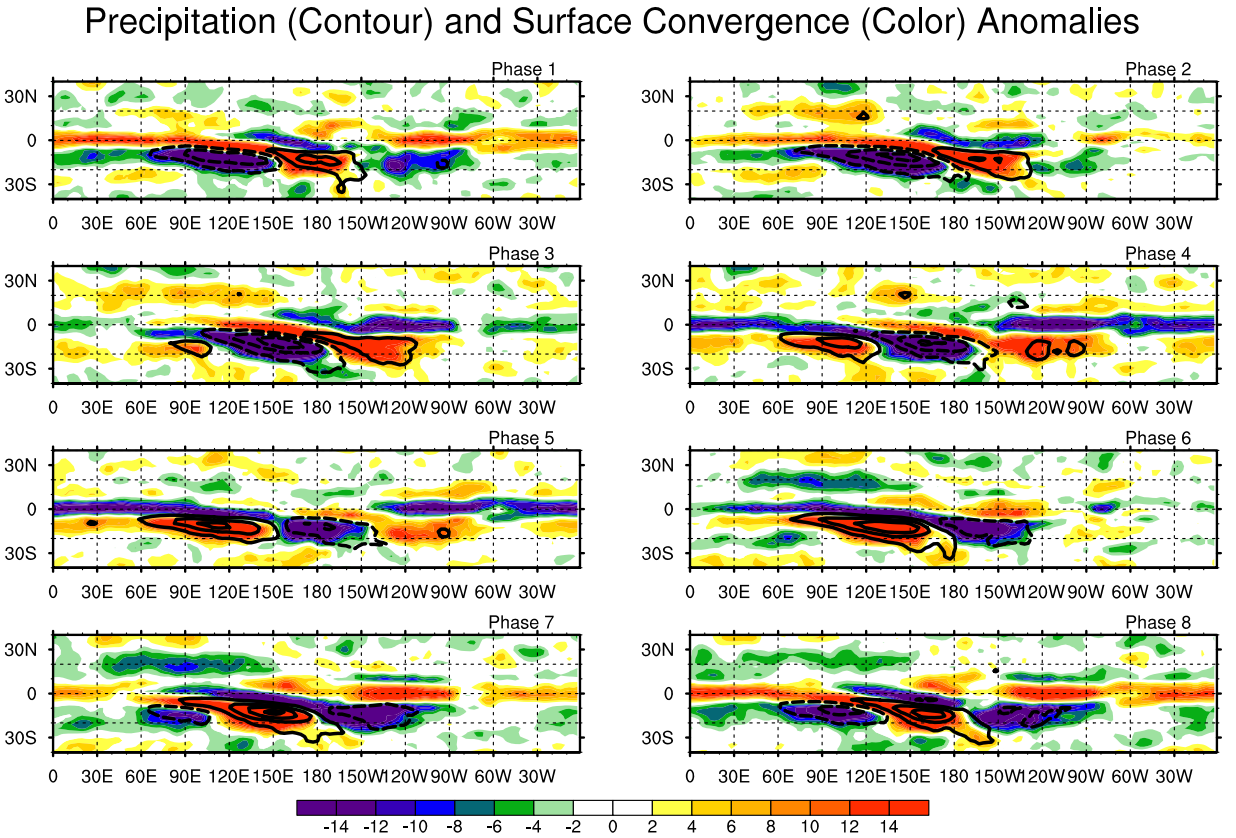

Figure 4. Composite surface convergence (color) and precipitation (contours) anomalies as a function of phase. The convergence anomalies have unit of 10^{-7} s^{-1}. The precipitation anomaly contour interval is 4 mm d^{-1}, starting at 2 mm d^{-1}. Negative contours are dashed.

3. Analysis of Moistening Processes in the Initiation Region

3.1. Composite Moisture and Dynamical Structures

We first redisplay the composite fields of Figure 3, except now we isolate the region where precipitation anomalies in the model are initiated. Figure 6 shows precipitation (contours) and precipitable water anomalies (colors) as a function of model MJO phase in the initiation region. Water vapor anomalies precede precipitation anomalies in a region centered near 60°E, 20°S, before expanding eastward and slightly northward at later times. A black box is placed around this region, which will be the focus for the moisture budget analysis to be shown later. Also notable in these plots are the equatorial water vapor anomalies and the Northern Hemisphere water vapor anomaly centered between 10°N and 20°N that occur in advance of precipitation anomalies in the western warm pool, but do not have to have any direct connection to the genesis of the resulting precipitation center. Phase 2 shows a nice example of this structure in advance of the onset of positive precipitation anomalies to the south of the equator. The off-equatorial moisture anomaly structures grow and expand eastward at later times. The Southern Hemisphere moisture center forms about 10° south of the observed boreal winter MJO initiation region, which is centered near 10°S, 60°E [*Zhao et al.*, 2013]. This dislocation from the region of observed initiation has implications for comparing the observed and model moisture budgets, as will be discussed later.

The moisture anomalies that straddle the equator and are prominent in Phases 2–3 and 6–7 intriguingly occur in regions where strong gyre-like circulations exist during MJO events [e.g., *Hendon and Salby*, 1994]. Figure 7 shows composite 850 hPa stream function anomalies (contours) and 400 hPa omega anomalies (colors) for Phases 2 and 6 of a model MJO lifecycle. During Phase 2, positive omega anomalies occur where the strong negative precipitation anomaly center occurs centered near 12°S, 140°E (Figures 3 and 6), with anomalies of the opposite sign during Phase 6. Precipitation anomaly centers of the opposite sign occur near the Dateline and further east (see also Figure 3). The stream function anomalies in Figure 7 resemble quadrapole vortices that result as a response to the MJO heating structure [e.g., *Hendon and Salby*, 1994;

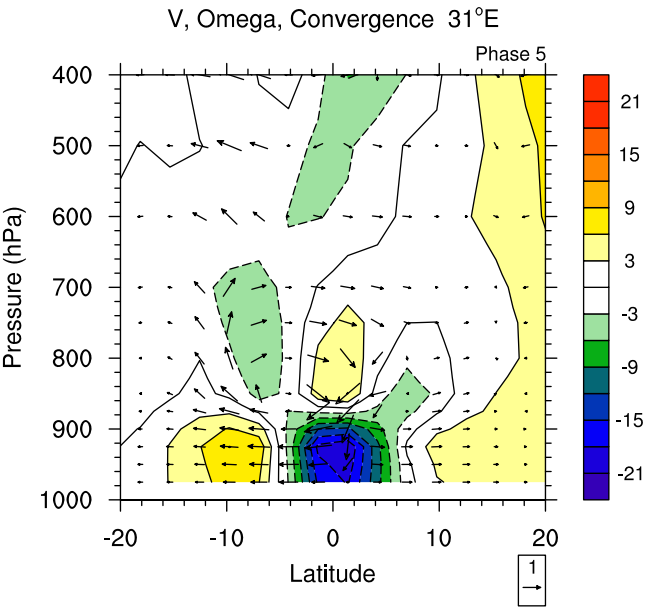

Figure 5. Pressure-latitude section of composite wind vector anomalies (meridional wind and omega) and convergence anomalies during Phase 5 at 31°E. The reference vector is shown in the bottom right, which is valid for both the meridional wind and omega. Units of meridional wind are m s^{-1}, and units of omega are 10^{-2} Pa s^{-1}. Divergence units are 10^{-7} s^{-1}.

Majda and Stechmann, 2009], and were previously suggested by *Zhao et al.* [2013] to play a role in the initiation of the next cycle of MJO convection in the Indian Ocean. Concentrating on the west side of the warm pool where model MJO initiation occurs, a comparison with Figure 6 indicates that positive moisture anomalies appear in association with the region of poleward flow on the west side of the gyres during Phase 2, and negative moisture anomalies appear in the equatorward flow on the west side of the gyres during Phase 6.

To demonstrate the likely formation mechanism for the gyres shown in Figure 7, we use the dry linear baroclinic model (LBM) of *Watanabe and Kimoto* [2000, 2001] forced with an idealized heat source meant to roughly approximate the MJO heating anomalies during Phase 2 (Figures 3 and 6). The LBM configuration consists of the primitive equations run at T42 resolution linearized about the CAM3 basic state. An idealized negative heating anomaly is centered at 12°S, 145°E having a Gaussian form in x and y with width in x 6 times that in y, which is the approximate horizontal shape of the strong downward motion patch in Figure 7 and the horizontal structure of coincident precipitation anomalies (Figures 3 and 6). The vertical heating structure is a half-sinusoid with a minimum at 450 hPa and an amplitude of 8 K d^{-1}, which represent the pressure and magnitude of peak negative MJO heating anomalies in the CAM3 (not shown). The sinusoidal vertical structure of the imposed forcing approximates the shape of the diabatic heating anomalies seen in the CAM3, although we find that the qualitative nature of the response shown below does not vary strongly with modest variations to the vertical heating structure. *Sobel and Maloney* [2012, 2013] argued that the MJO horizontal flow can be modeled as a steady balanced response to the diabatic heating field under conditions of weak tropical temperature gradients, and hence the balanced flow response in the LBM should be consistent with such considerations.

Figure 8 indicates that the LBM forms gyre-like circulations in the lower troposphere in response to the imposed heat source, analogous to those shown in Figure 7. Figure 8 also shows the anomalous vertical velocity field at 400 hPa produced by the LBM, indicating descent in the region of imposed forcing, and ascent that maximizes in the poleward flow on the west flank of the gyre-like circulations, consistent with the regions of ascent associated with forced Rossby gyres found in previous idealized modeling studies [e.g., *Heckley and Gill*, 1984]. These basic features are also seen in the Phase 2 GCM composites of Figure 7. We might expect the upward motion on the west side of the gyres to moisten the atmosphere through ascent, and horizontal advection to moisten by advection across the mean meridional humidity gradient that increases toward the equator, hypotheses we will explore in more detail in the moisture budget analysis that follows. We caution that we would not expect a quantitative comparison between the LBM and GCM vertical velocity anomalies to be valid since the LBM we use does not include interactive diabatic heating that can enhance the vertical velocity features shown. However, this simple model gets the correct qualitative sense of the vertical velocity and stream function response seen in Figure 7.

3.2. Moisture Budget

We will now discuss the impact of these gyre-like circulations on the moisture budget in the initiation region. The vertically integrated moisture budget can be approximated as

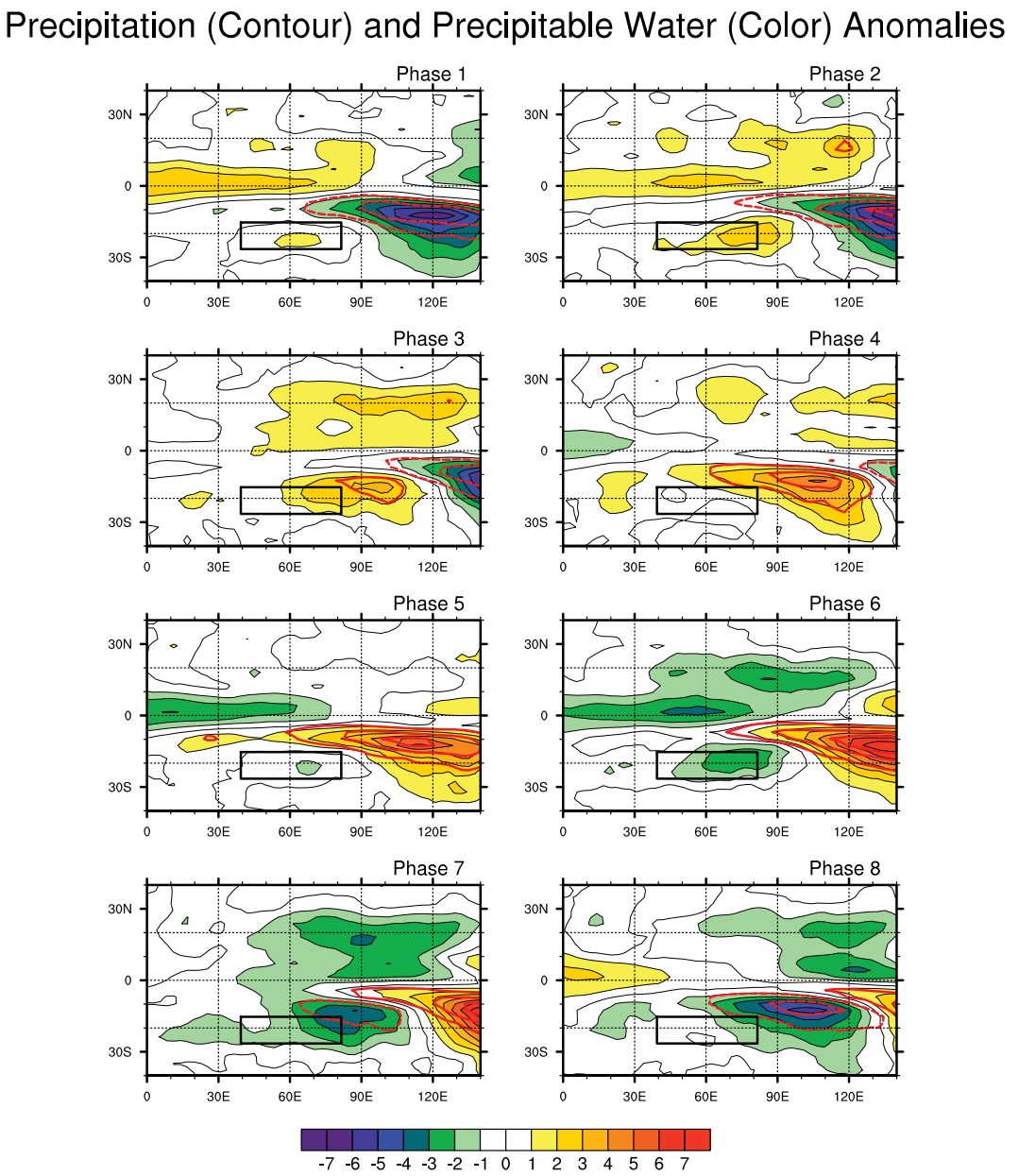

Figure 6. As in Figure 3, except that the initiation region is isolated. The black box in each figure represents the domain that will be used to assess the initiation region moisture budget in Figures 10 and 11 below.

$$\left\langle \frac{\partial q}{\partial t} \right\rangle = -\left\langle \omega \frac{\partial q}{\partial p} \right\rangle - \langle \vec{v} \cdot \nabla q \rangle + E - P. \tag{1}$$

Here ω represents pressure velocity, $\vec{v}$ is the horizontal wind vector, q is specific humidity, p is pressure, P is total precipitation, and E is surface evaporation. Brackets represent a vertical integral from the surface to 100 hPa. This budget neglects storage of condensate in the form of cloud water and ice, which is assumed to be small.

First, to get a sense of the possible impact of the vertical velocity anomalies on moistening, Figure 9 shows Phases 2 and 6 composite anomalies of $\langle -\omega \frac{\partial q}{\partial p} \rangle - P$. This quantity was shown by *Wolding and Maloney* [2015] to be a vertically integrated version of the "column process" of *Chikira* [2014] that represents the net effect of diabatic processes on the moisture budget at a given vertical level (see also the discussion of *Janiga and Zhang* [2015]), where P is approximately equal to net condensation in the column. The quantity

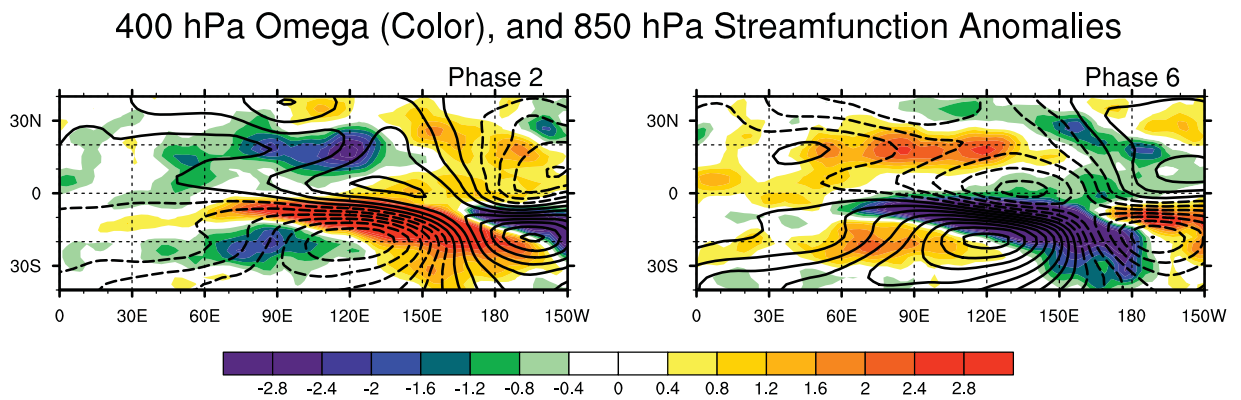

Figure 7. Composite 400 hPa omega anomalies (color) and 850 hPa stream function anomalies (contours) during Phases 2 and 6. Units of omega are 10^{-2} Pa s^{-1}. The stream function anomaly contour interval is 1×10^6 m^2 s^{-1}, starting at 0.5×10^6 m^2 s^{-1}. Negative contours are dashed.

$\left\langle -\omega \frac{\partial q}{\partial p} \right\rangle - P$ thus accounts for the ability of vertical advection to moisten or dry the atmosphere after accounting for associated condensational tendencies that occur in regions of anomalous vertical velocity. Figure 9 shows that net moistening due to the column process during Phase 2 occurs in the same off-equatorial regions as ascent is occurring in the composite of Figure 7, with analogous opposite signed anomalies during Phase 6. In particular, Phase 2 moistening is located near the Southern Hemisphere MJO initiation region (see Figure 6), supporting the hypothesis that the descent in that region contributes to drying. Horizontal advection anomalies exist in a broadly similar pattern to $\left\langle -\omega \frac{\partial q}{\partial p} \right\rangle - P$ anomalies in regions of poleward or equatorward flow associated with the gyres shown in Figure 7 (not shown here). The particular contributions of various moistening processes to the moisture budget of the initiation region defined by the box in Figure 6 will now be more precisely quantified.

Figure 10 shows anomalous precipitable water and P (Figure 10a), and anomalous moisture budget terms (Figure 10b) averaged over the initiation region 40°E–80°E, 17.5°S–25°S (averaging box in Figure 6). Within this initiation region, positive precipitable water anomalies first form in Phase 1, and then maximize during Phases 2 and 3. Likewise, negative humidity anomalies initiate in Phase 5, and maximize in Phases 6 and 7. P anomalies approximately track the behavior of precipitable water anomalies. Under the assumption of cyclic phase progression from Phases 8 to 1 (a good assumption, given the statistics on successive events described above), horizontal advection and $\left\langle -\omega \frac{\partial q}{\partial p} \right\rangle - P$ anomalies are both of comparable importance for driving a moisture tendency in the initiation region, although horizontal advection anomalies lead those associated with $\left\langle -\omega \frac{\partial q}{\partial p} \right\rangle - P$. The column process $\left\langle -\omega \frac{\partial q}{\partial p} \right\rangle - P$ shows a positive covariance with moisture anomalies, and may thus also play an important role in maintaining the growing MJO moisture anomaly in the initiation region. The higher amplitude of the precipitation anomalies (that strongly damp the moisture anomaly) relative to the terms in the moisture budget of Figure 10b highlights the importance of vertical advection that is a response to local and remote heating anomalies for maintaining the moisture anomalies coincident with precipitation. While speculated above that anomalous meridional flow acting across the mean humidity gradient could be a major agent of horizontal advective moistening tendencies, this contention will be explored in more detail in the next paragraph. As discussed above, regions of moistening during Phases 1–3 associated with $\left\langle -\omega \frac{\partial q}{\partial p} \right\rangle - P$ are consistent with the ascent region of the anticyclonic low-level Rossby gyre forced by the previous phase of MJO suppressed convection. *Ruppert and Johnson* [2015] argued that $\left\langle -\omega \frac{\partial q}{\partial p} \right\rangle - P$ served

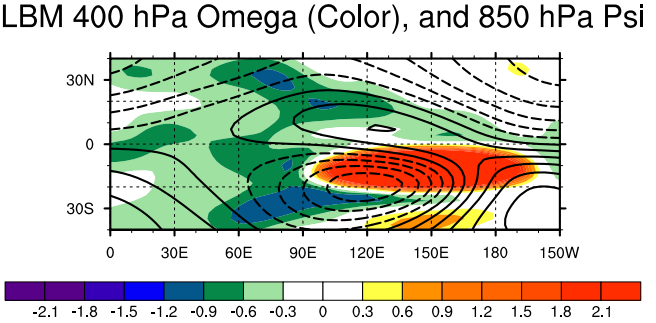

Figure 8. Four hundred hectopascal omega anomalies (color) and 850 hPa stream function anomalies (contours) derived from the linear baroclinic model. Units of omega are 10^{-2} Pa s^{-1}. The stream function anomaly contour interval is 1.5×10^6 m^2 s^{-1}, starting at 0.75×10^6 m^2 s^{-1}. Negative contours are dashed.

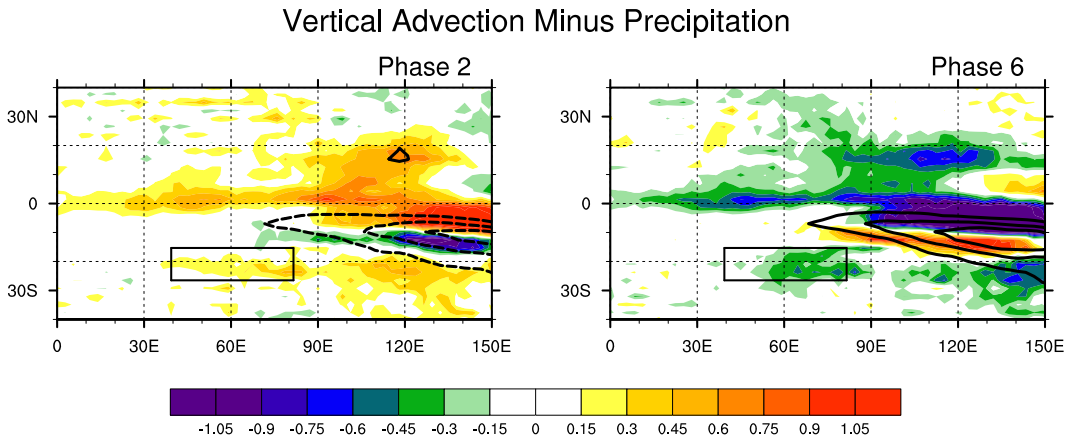

Figure 9. Composite vertical moisture advection minus precipitation anomalies (color) and precipitation anomalies (contours) for the initiation region during Phases 2 and 6. Units of moisture convergence minus precipitation are mm d^{-1}. The precipitation anomaly contour interval is 4 mm d^{-1}, starting at 2 mm d^{-1}, with negative contours dashed. The initiation region as described in the text is also shown as a box.

as a major moistening mechanism during the preonset phase of MJO events during the DYNAMO time period, with invigoration of the vertical advection signal due to radiative feedbacks. Surface evaporation (*E*) provides only modest contributions to the anomalous moisture budget.

We note that the moisture budget transitions to resemble that of mature model MJO events documented in *Maloney et al*. [2010, Figure 13] by the time convection and moisture anomalies have reached 90°E (not shown here). For mature events, the column process is weakly in opposition to column moisture and precipitation anomalies in the area average, and the surface latent heat flux anomalies are of larger magnitude than the column process and exhibit a positive covariance with column moisture anomalies. This suggests that the moistening processes at initiation are different than those that maintain mature model MJO events. MJO maintenance processes may be established after the moisture and precipitation anomalies reach stronger mean low-level westerly flow near 90°E and eastward [see *Maloney et al*., 2010, Figure 2].

As in *Maloney* [2009], we conduct a linearization of horizontal advection anomalies such that

$$-(\vec{v}\cdot\nabla q)_{ISO} \approx -(\bar{\vec{v}}\cdot\nabla q')_{ISO} - (\vec{v}'\cdot\nabla\bar{q})_{ISO} - (\vec{v}'\cdot\nabla q')_{ISO}. \quad (2)$$

Overbars represent a 51 day running mean that approximately spans the length of model MJO events, primes represent deviations from that mean, and the subscript ISO represents application of a 20–100 day band-pass filter, which is applied after construction of the linearized equations. The results of this partitioning are shown in Figure 11, with the decomposition for vertically integrated meridional advection shown in the top plot, and for zonal advection shown in the bottom plot. Meridional advection clearly dominates the horizontal advection signal, perhaps not surprising given the off-equatorial initiation region and the strong influence from meridional flow associated with Rossby gyres in that region (e.g., Figure 7). The dominance of meridional advection in the model is different than that suggested in budgets from some observational studies, where the zonal advection appears to be at least as important as meridional advection in the Indian Ocean initiation region [e.g., *Kiranmayi and Maloney*, 2011a; *Zhao et al*., 2013; *Sobel et al*., 2014; *Kim et al*., 2014]. However, *Sobel et al*. [2014] note that a significant portion of the zonal moisture advection signal in the Indian Ocean during MJO events may start as air being advected meridionally around Rossby gyres and being entrained into the equatorial region, a feature also discussed by *Ruppert and Johnson* [2015]. Further, the interpretation of the partitioning of zonal versus meridional advection may also depend on the latitude averaging band used [e.g., *Wolding*, 2013].

Figure 11a indicates that the mix of processes responsible for moistening and drying in the initiation region due to meridional advection are complicated. The progression of terms will be described here in advance of the development of positive moisture anomalies, although a similar progression but with opposite sign holds for the development of negative moisture anomalies. Moistening first occurs in association with the term $-\left(v'\frac{\partial q'}{\partial y}\right)_{ISO}$ that peaks during Phases 6 and 7. A more detailed examination of this term (not shown)

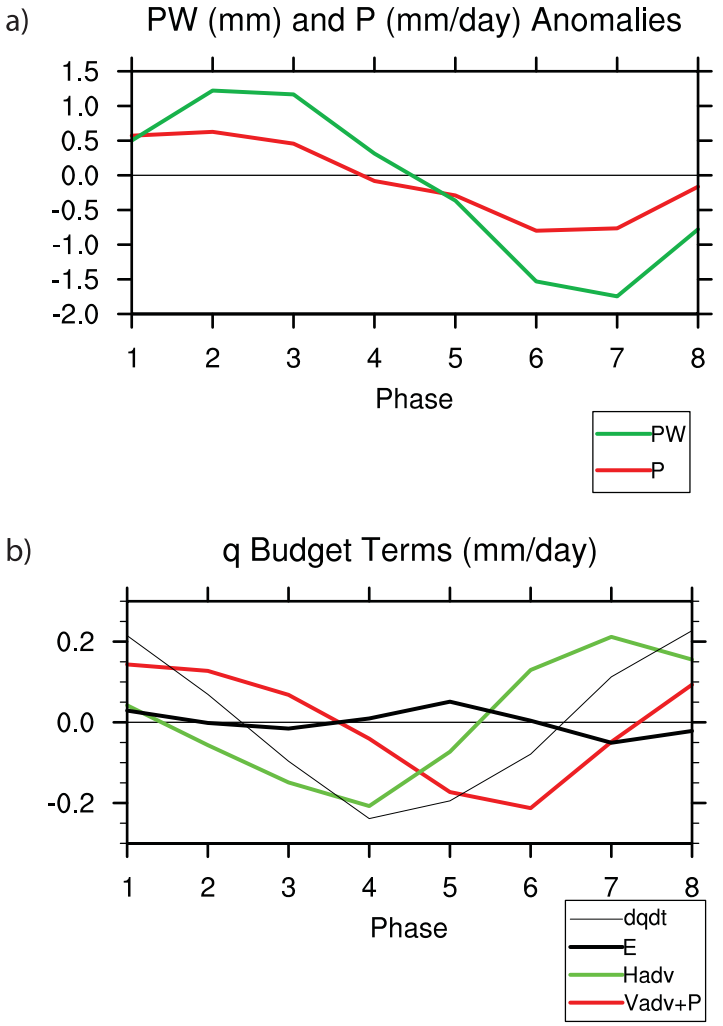

Figure 10. (a) Composite vertically integrated precipitable water anomalies and precipitation anomalies as a function of phase averaged over the region defined in Figures 6 and 9 and (b) anomalous vertically integrated moisture budget terms averaged for the same area.

indicates that this term is associated both with MJO-time scale flow anomalies acting across the anomalous MJO moisture gradient (e.g., examine the stream function anomalies in Figure 7 and how associated northerly flow anomalies would operate on the moisture gradients in Figure 6), and through the actions of synoptic-time scale rotational disturbances mixing across the anomalous moisture gradient and weakening the associated moisture anomalies, as has been hypothesized by previous modeling studies [*Maloney*, 2009; *Maloney et al*., 2010; *Andersen and Kuang*, 2012]. The importance of synoptic scale disturbances to the Indian Ocean MJO moisture has also been documented in some reanalysis studies [e.g., *Wolding*, 2013], although possibly with a weaker influence than in the model used here [e.g., *Zhao et al*., 2013; *Kim et al*., 2014].

During Phases 8 to 2, the action of the anomalous MJO flow acting on the mean meridional moisture gradient $-\left(v'\frac{\partial \bar{q}}{\partial y}\right)_{ISO}$ moistens the atmosphere, consistent with a role for anomalous Rossby gyres in moistening the atmosphere in advance of MJO initiation. The MJO flow anomalies associated with Rossby-gyre-like circulations acting on the mean moisture gradient have been previously proposed as a moistening mechanism in the MJO initiation region in observational studies [e.g., *Zhao et al*., 2013]. The term $-\left(\bar{v}\frac{\partial q'}{\partial y}\right)_{ISO}$ is also not negligible, contributing to moistening during Phases 6–8 and is associated with the model's climatological southerly flow in this region [see *Maloney et al*., 2010, Figure 2a] acting on the anomalous MJO moisture gradient that is shown in Figure 6.

As a summary, our budget analysis indicates that the moistening process in the MJO initiation region is strongly regulated by the Rossby gyres forced by the previous cycle of suppressed MJO convection through

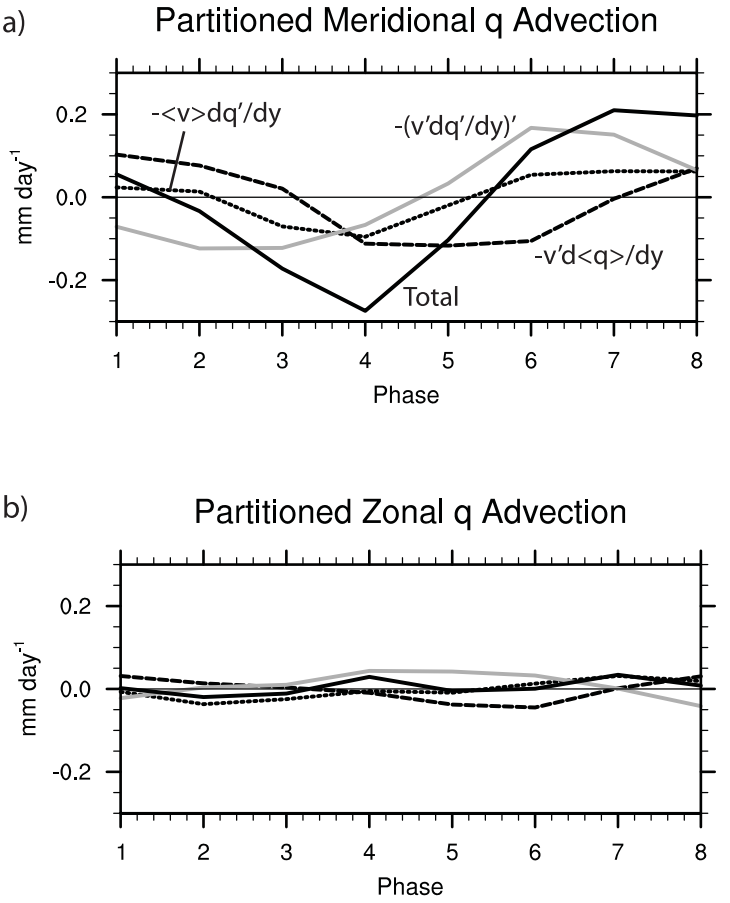

Figure 11. (a) Composite partitioned vertically integrated perturbation meridional *q* advection averaged within the region defined in Figures 6 and 9 as a function of phase. The definition of partitioned terms is indicated on the plot. (b) Same as Figure 11a, except for zonal advection. The line convention is analogous to that in Figure 11a.

both column process (net effect of vertical advection and condensational drying) and horizontal advection anomalies. However, the results of Figures 3 and 4 above also suggest that variations in ascent and moistening associated with circumnavigating Kelvin waves may also influence the growing convective signal near and to the east of the initiation region. We next investigate the importance of circumnavigating Kelvin waves to MJO events and their initiation.

4. Damping Kelvin Wave Circumnavigation

Figures 3 and 6 and the associated analysis above indicates that a circumnavigating Kelvin wave signal imprints equatorial moisture anomalies in advance of the initiation of model MJO events. We cannot rule out based on the analysis so far that this imprinted moisture anomaly has a significant indirect impact on the initiation of the model MJO, for example, by modifying the moisture anomaly field that can regulate moistening processes in the initiation region by the terms $-\left(v'\frac{\partial q'}{\partial y}\right)_{ISO}$ or $-\left(\bar{v}\frac{\partial q'}{\partial y}\right)_{ISO}$. A key question is whether any changes to model MJO behavior, including the regularity or amplitude of MJO events, occur by suppressing equatorial circumnavigation.

To suppress Kelvin wave circumnavigation, we redo the control experiment, except that now a sponge region is applied within the region 60°W–0°W, 20°N–20°S that damps surface pressure, dry static energy, horizontal winds, and specific humidity at all vertical levels toward the climatology of the control simulation with a time scale of 1 day. This method is identical to that employed in *Rydbeck et al*. [2013] to isolate the east Pacific warm pool from atmospheric Kelvin waves forced by the MJO in the west Pacific. The simulation with Kelvin wave circumnavigation suppressed will be referred to as the "sponge" simulation. The 1 day

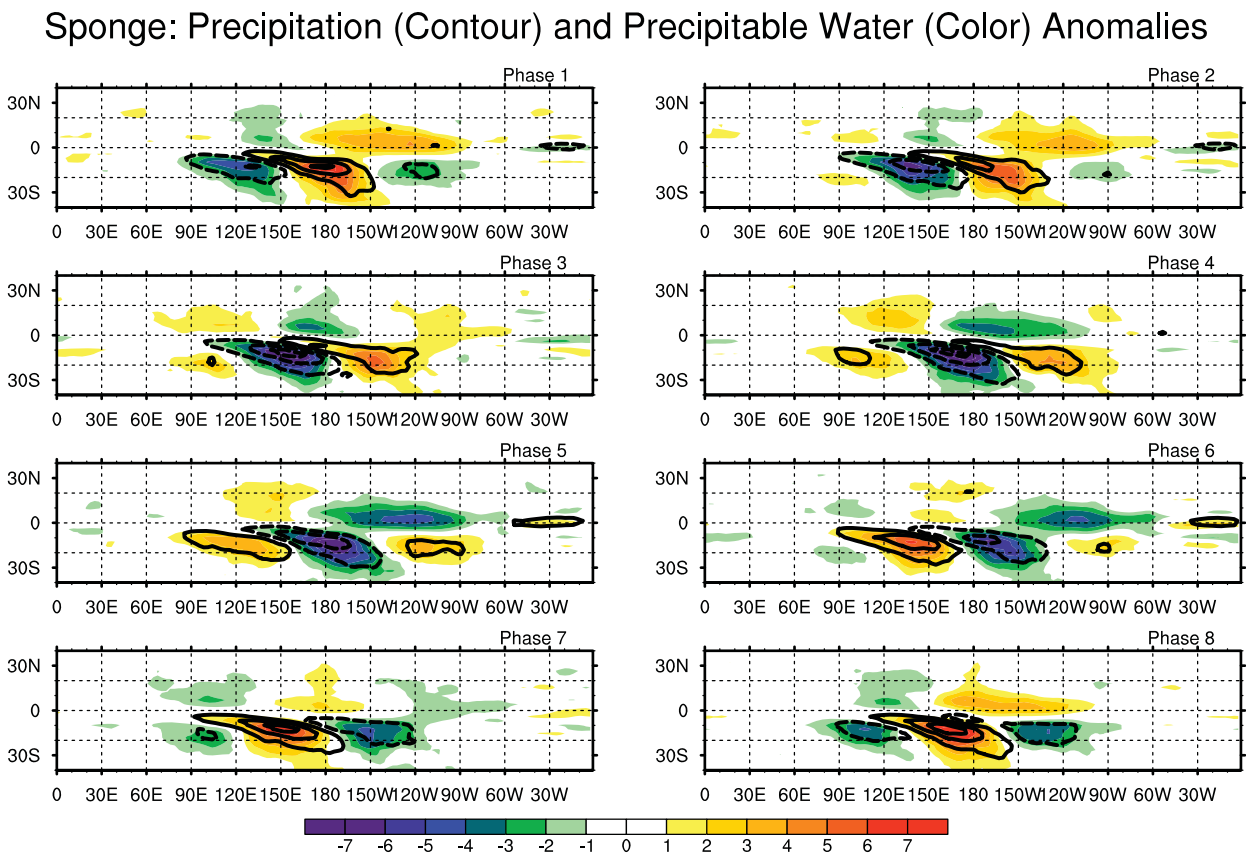

Figure 12. As in Figure 3, except for the sponge experiment.

relaxation time scale that we use represents a compromise between a shorter relaxation time scale (e.g., 6 h) that would completely remove circumnavigating waves but might provide a greater shock to the model, and a longer 2 day relaxation time scale that would minimize model shock but not as effectively damp Kelvin wave circumnavigation. We have strategically placed the damping region away from the region of MJO convective activity to minimize any adverse effects resulting from the relatively short 1 day relaxation time. Nevertheless, we cannot completely rule out that the short adjustment time used here may produce some unintended consequences in the model, although our experiment design tries to minimize these issues.

Events in the sponge simulation are just as regular as in the control simulation, with 78% of MJO events that initiate in the western warm pool immediately preceded by another MJO event (compared to 79% in the control simulation). A space-time spectral analysis also indicates no significant changes to the temporal and spatial characteristics of the variability (not shown). This result suggests that circumnavigation is not necessary for producing the regular MJO variability in the aquaplanet model, and that factors such as Rossby gyres associated with the previous cycle of MJO suppressed convection may be more important for generating this regularity. *Ray and Li* [2013] found a similar result in a GCM with realistic continental configurations in which a damping region was added to tropical Atlantic to suppress Kelvin wave circumnavigation.

Figure 12 shows a similar composite lifecycle of precipitation and precipitable water anomalies for the sponge simulation as was shown for the control simulation in Figure 3. A composite basis was generated using complex EOF analysis as in the control simulation. In most respects, the composite evolution of MJO events in the sponge simulation is similar to that of the control, with a couple of notable exceptions. One notable difference is that the amplitude of moisture and precipitation anomalies is reduced to the west of about 140°E, as will be quantified in more detail below. Another exception is the lack of a narrow

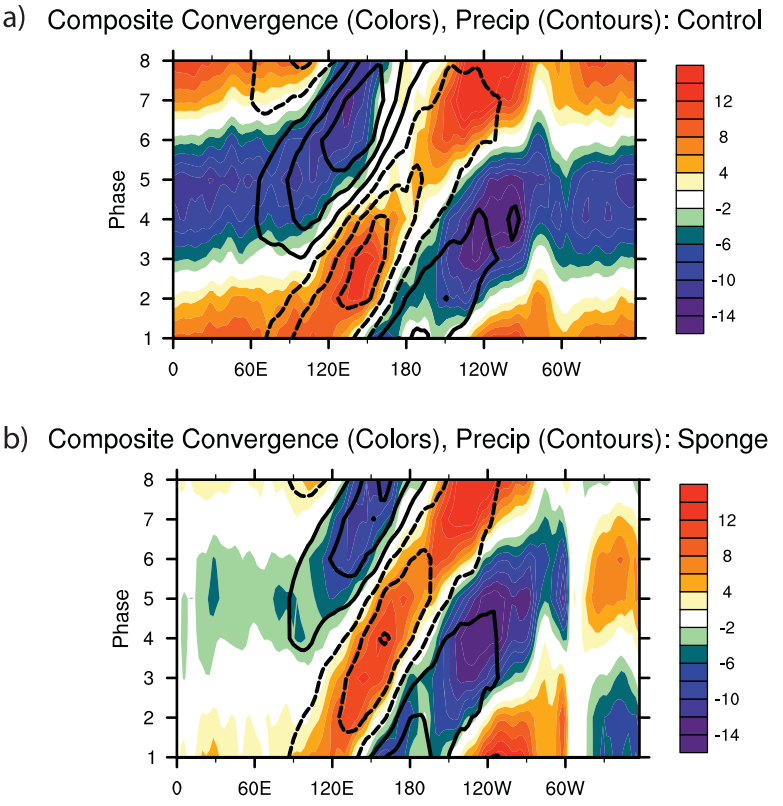

Figure 13. Composite 5°N–5°S averaged surface convergence (colors) and 0°S–20°S averaged precipitation (contours) anomalies as a function of phase and longitude for the (a) control simulation and (b) sponge simulation. The precipitation contour interval is 2 mm d^{-1}, starting at 1 mm d^{-1}. The units of convergence are 10^{-7} s^{-1}.

circumnavigating equatorial moisture signal that was associated with moistening and drying by the circumnavigating Kelvin wave forced by MJO heating in the control simulation (compare to Figure 3). Figure 13 shows that suppression of a circumnavigating equatorial convergence anomaly signal accompanies the suppression of equatorial moisture anomalies, providing more evidence that Kelvin wave circumnavigation in the sponge simulation is strongly suppressed.

Figure 14 shows composite *P* and precipitable water anomalies as a function of longitude averaged from 0°S to 20°S for the control and sponge simulations, demonstrating similar composite behavior between the two simulations, except for the weaker amplitude variability in the sponge simulation to the west of 150°E. Figure 14c provides a more quantitative assessment of the amplitude difference between the control and sponge simulations as a function of longitude. A precipitation amplitude is defined by taking one-half the difference between the maximum and minimum of the composite precipitation anomalies at each longitude as determined from Figures 14a and 14b. Figure 14c shows that the amplitude of MJO precipitation variability is similar between the control and sponge simulations to the east of 150°E, but the amplitude in the sponge simulation is notably reduced relative to the control to the west of 150°E. The amplitude at the longitude of strongest MJO activity in the control simulation (near 140°E) is reduced by about 17% in the sponge simulation. Hence, while the regularity of MJO events in the model does not change when suppressing Kelvin wave propagation, suppressing Kelvin wave propagation does appear to weaken the amplitude of the model MJO in the western part of the warm pool. Because circumnavigating Kelvin waves have been observed to influence the MJO initiation region even after propagating past substantial topographic obstacles [e.g., *Matthews*, 2008], MJO amplitude in the real world may be influenced by the occasional influence from circumnavigating waves forced by the previous cycle of MJO convection.

Although the regularity of MJO events in the sponge simulation is unchanged, the amplitude changes in the western part of the warm pool deserve some discussion. One possibility for the decrease in amplitude is

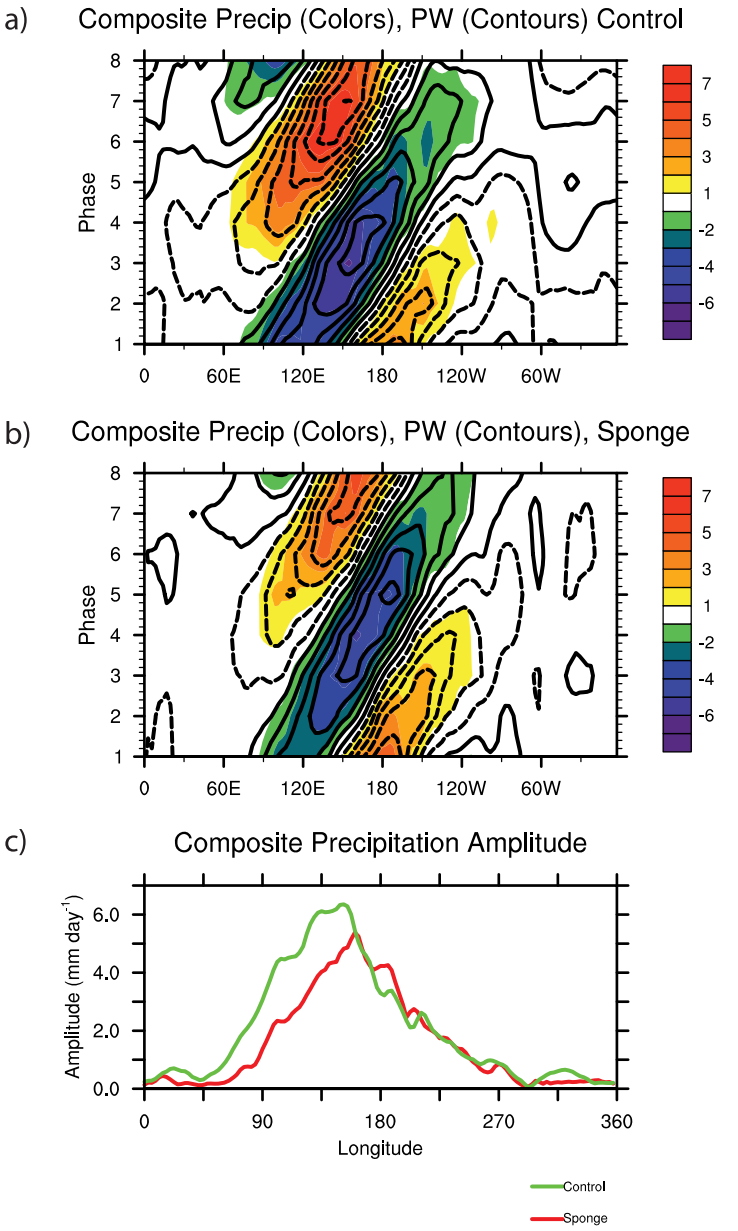

Figure 14. Composite 0°S–20°S averaged precipitation (colors) and precipitable water (contours) anomalies as a function of phase and longitude for the (a) control simulation and (b) sponge simulation, and (c) the amplitude of precipitation anomalies in the control and sponge simulations. The precipitable water contour interval is 0.8 mm, starting at 0.4 mm. The precipitation units are mm d^{-1}.

that the equatorial convergence-induced moisture anomaly (as shown in Phases 1–2, 5–6 of Figure 6) may somehow indirectly help to maintain the same-signed off-equatorial moisture anomaly through changing the anomalous moisture gradient on which flow anomalies act, or through some other means. A comparison of partitioned moisture budgets (as in Figure 11) between the control and sponge simulations (not shown here) does not provide compelling evidence to support this view, however. Having an enhanced equatorial moisture signal generated by the circumnavigating Kelvin wave in the vicinity of the off-equatorial moisture anomaly may effectively increase the scale of the moist region. This broader moist region may support convection anomalies over a wider region, allowing scale-selective feedbacks to initiate. The effect of the circumnavigating Kelvin waves on off-equatorial boundary layer convergence, and the subsequent influence on tropospheric moistening, is another potential means through which

circumnavigating Kelvin waves can support moisture and convection anomalies. Figure 5 shows the presence of an off-equatorial convergence anomaly signature with the circumnavigating Kelvin wave that is out of phase with the equatorial signal. Figure 4 shows that this off-equatorial convergence anomaly signature propagates into and affects the western warm pool at about the same time as the growth period of positive convection anomalies during Phases 3–5 in the control simulation, with anomalies of the opposite sign impinging on the warm pool during Phases 8 and 1. The relative role of vertical advection in the moisture budget compared to other terms in the MJO initiation region and areas further east is strongly diminished in the sponge simulation compared to the control simulation, supporting this contention. Without the support from this circumnavigating signal, it takes longer for the amplitude of moisture and convection anomalies in the sponge simulation to match that of the control simulation as the convective complex propagates eastward. We note that an important role for circumnavigating Kelvin waves in supporting the next cycle of MJO convection is broadly consistent with the aquaplanet results of *Haertel et al*. [2014], although the details of the proposed mechanism differ significantly between our study and theirs. As in their study, a circumnavigating Kelvin wave front with cold equatorial tropospheric anomalies arrives during the growth phase of convection in the western warm pool, although the off-equatorial nature of initial convective anomalies in our model likely minimizes the direct influence of these equatorial cold anomalies on MJO initiation. The effect of the frictionally induced surface convergence field associated with these circumnavigating waves is likely more important in our model.

The conclusions drawn from our sponge simulation have significant caveats. It cannot be ruled out that mean state changes produced in the sponge simulations are contributing to diminished MJO amplitude in the western part of the warm pool. As shown in *Maloney et al*. [2010], the control simulation contains substantial low-level mean westerlies across the warm pool, and the magnitude of these mean westerlies is diminished in the sponge simulation (not shown). Previous studies have cited a connection between mean state westerlies in a model and the ability to produce a realistic amplitude MJO [e.g., *Inness et al*., 2003; *Maloney and Sobel*, 2004; *Ray et al*., 2012]. *Maloney and Sobel* [2004] argued that the mean winds significantly affect the magnitude of surface flux anomalies and phasing of surface latent heat flux anomalies relative to precipitation anomalies, which can affect the ability to destabilize the MJO. The model used here contains an MJO that is particularly sensitive to wind-evaporation feedbacks as compared to other destabilization mechanisms [*Maloney et al*., 2010; *Kiranmayi and Maloney*, 2011b]. It is unclear why the mean state westerly flow is weaker in the sponge simulation. One possibility is simply that the weaker mean westerlies in the western warm pool are a result of the reduced MJO activity rather than a cause, due to the rectification of the MJO flow onto longer time scales, and reduced eddy momentum fluxes toward the equator that would weaken the westerly flow [e.g., *Shell and Held*, 2004]. However, another possibility is that the design of our sponge experiments, with a damping region from 60°W to 0°W, 20°N to 20°S, may itself be directly damping equatorward eddy momentum fluxes and hence weakening the westerly flow in the eastern part of the warm pool, which would then weaken MJO activity. Neither of these possibilities can be discounted. Mean precipitation and intraseasonal precipitation variance both decrease in the western part of the warm pool in the sponge experiment relative to the control, further supporting substantial interactions between the mean state and the model MJO, although the direction of causality is difficult to disentangle. *Ray and Li* [2013] did not find significant changes in either Indo-Pacific warm pool mean precipitation or MJO strength when suppressing Kelvin wave circumnavigation through an Atlantic damping region.

5. Conclusions

This study examined processes associated with MJO initiation in an aquaplanet GCM with strong and regular MJO-like variability. An idealized SST distribution is used having a simple tropical warm pool centered slightly south of the equator. The control version of the model produces MJO-like activity that is stronger and more regular than observed, with 79% of MJO events that initiate on the western side of the warm pool being immediately preceded by an existing significant MJO event. Hence, the dynamics of MJO initiation in the model are dominated by interactions with preceding events. *Matthews* [2008] classified 60% of observed events as being similarly successive.

MJO initiation in the model occurs to the south of the equator in a region strongly influenced by Rossby gyres produced by suppressed MJO convective anomalies further east. Previous work showed that understanding the processes controlling the tropospheric water vapor field is key to understanding the MJO dynamics in this model [*Maloney et al*., 2010]. The moisture tendencies associated with column processes and horizontal advection dominate moistening processes in the initiation region under influence from these Rossby gyre circulations, consistent with previous results by *Zhao et al*. [2013], although the model initiation region is more off-equatorial than observed and hence it is perhaps expected that Rossby gyres would play a key role in initiation in this model. Anomalous vertical advective moistening exceeds anomalous moisture removal by precipitation in advance of MJO initiation, consistent with moistening by the column process of *Chikira* [2014]. Such moistening is coincident with the region of upward motion associated with lower tropospheric poleward flow in Rossby gyres forced as a response to suppressed near-equatorial heating to the east of the initiation region. Zonal advection is negligible to moistening in the initiation region, unlike observations where it forms a significant component of the total horizontal advection [e.g., *Kiranmayi and Maloney*, 2011a, 2011b; *Zhao et al*., 2013; *Sobel et al*., 2014; *Wolding*, 2013]. Partitioning of meridional advection shows that the anomalous meridional MJO flow acting on the climatological moisture gradient is important for regulating horizontal moisture advection in advance of MJO initiation, although other terms make similarly large contributions.

The control simulation exhibits strong moisture and low-level convergence anomalies consistent with circumnavigating Kelvin waves forced by MJO heating. A simulation was conducted in which circumnavigating Kelvin waves forced in the eastern part of the warm pool were suppressed by a damping region in the Western Hemisphere. In this "sponge" simulation, MJO events are just as regular as in the control simulation, but the amplitude of MJO variability, especially in the western part of the warm pool, is reduced relative to the control simulation. It is hypothesized that suppression of off-equatorial convergence anomalies associated with these circumnavigating Kelvin wave signatures may remove a means of supporting convective anomalies in the model via anomalous vertical moisture advection. We cannot rule out that mean state changes in the sponge simulation also contribute to the reduction in MJO amplitude in the model, especially weakening of low-level mean state westerlies in the western part of the warm pool. However, it is unclear whether the reduction in mean state westerlies is a result or a cause of the reduction in MJO activity.

An obvious outstanding question of this research is the degree to which the conclusions derived here apply to the real world, given the highly idealized aquaplanet setup of the model used. While our conclusions are broadly consistent with recent observational studies [e.g., *Zhao et al*., 2013], the details differ from observations due to the highly idealized nature of the modeling setup. For example, the impact of circumnavigating Kelvin waves on the amplitude of MJO activity in the model may be too strong, given the lack of intervening physical barriers such as the Andes. Future model experiments should use a more realistic setup to assess the importance of circumnavigating Kelvin waves to the MJO and its initiation [e.g., *Ray and Li*, 2013]. The initiation location of MJO convection in the model used here is also too far south. We also note that observed MJO convective activity has a local minimum at longitudes of the Maritime Continent [e.g., *Sobel et al*., 2010; *Peatman et al*., 2014]. Our aquaplanet model does not exhibit an MJO amplitude minimum at such longitudes, and Figure 7 shows that heating anomalies at longitudes characteristic of the Maritime Continent are responsible for Rossby gyre formation that aids moistening in the model MJO initiation region. While observed studies also suggest the importance of Rossby gyres to MJO initiation [e.g., *Zhao et al*., 2013], the observed MJO heating amplitude minimum in the Maritime Continent region suggests that further model experiments with realistic land-ocean distributions should be conducted to test the robustness of this mechanism.

The model dependence of these results should also be tested. For example, MJO destabilization in the current model may have too strong of a dependence on wind-evaporation feedbacks relative to radiative feedbacks [e.g., *Maloney*, 2009; *Maloney et al*., 2010; *Kiranmayi and Maloney*, 2011b], making the model MJO potentially too sensitive to changes in the basic state low-level wind such as occurred in the sponge experiment. Using a model with more realistic interactions between convection, radiation, and the atmospheric boundary layer, such as the superparameterized CAM (SP-CAM) [e.g., *Benedict and Randall*, 2009], would be a fruitful way to test some of the findings derived here.

Acknowledgments
Three reviewers provided insightful comments that led to significant improvements to the manuscript. Data from the simulations described in this manuscript are archived on the NCAR HPSS and are freely available to all investigators and can be obtained from the lead author (E.M.). All other data and code in the manuscript can also be obtained from the lead author. The authors thank Jeffrey Shaman for supplying the code to implement damping of circumnavigating Kelvin waves. This work was supported by award NA13OAR4310163 from NOAA, U.S. Department of Commerce, by the Climate and Large-Scale Dynamics Program of the National Science Foundation under grants AGS-1062161 and AGS-1441916, and the Science and Technology Center for Multi-Scale Modeling of Atmospheric Processes, managed by Colorado State University under Cooperative Agreement ATM-0425247. The statements, findings, conclusions, and recommendations do not necessarily reflect the views of NOAA or NSF.

References

Andersen, J. A., and Z. Kuang (2012), Moist static energy budget of MJO-like disturbances in the atmosphere of a zonally symmetric aquaplanet, *J. Clim.*, *25*, 2782–2804.

Bellenger, H., K. Yoneyama, M. Katsumata, T. Nishizawa, K. Yasunaga, and R. Shirooka (2015), Observation of moisture tendencies related to shallow convection, *J. Atmos. Sci.*, *72*, 641–659.

Benedict, J. J., and D. A. Randall (2007), Observed characteristics of the MJO relative to maximum rainfall, *J. Atmos. Sci.*, *64*, 2332–2354, doi:10.1175/JAS3968.1.

Benedict, J. J., and D. A. Randall (2009), Structure of the Madden–Julian Oscillation in the superparameterized CAM, *J. Atmos. Sci.*, *66*, 3277–3296.

Bladé, I., and D. L. Hartmann (1993), Tropical intraseasonal oscillations in a simple nonlinear model, *J. Atmos. Sci.*, *50*, 2922–2939.

Chikira, M. (2014), Eastward-propagating intraseasonal oscillation represented by Chikira–Sugiyama cumulus parameterization. Part II: Understanding moisture variation under weak temperature gradient balance, *J. Atmos. Sci.*, *71*, 615–639.

de Szoeke, S. P., J. B. Edson, J. R. Marion, and C. W. Fairall (2015), The MJO and air-sea interaction in TOGA COARE and DYNAMO, *J. Clim.*, *28*, 597–622.

DeMott, C. A., C. Stan, D. A. Randall, and M. D. Branson (2014), Intraseasonal variability in coupled GCMs: The roles of ocean feedbacks and model physics, *J. Clim.*, *27*, 4970–4995.

Fu, X., W. Wang, J.-Y. Lee, B. Wang, K. Kikuchi, J. Xu, J. Li, and S. Weaver (2015), Distinctive roles of air-sea coupling on different MJO events: A new perspective revealed from the DYNAMO/CINDY field campaign, *Mon. Weather Rev.*, *143*, 794–812, doi:10.1175/MWR-D-14-00221.1.

Gonzalez, A. O., and G. Mora Rojas (2014), Balanced dynamics of deep and shallow Hadley circulations in the tropics, *J. Adv. Model. Earth Syst.*, *6*, 777–804, doi:10.1002/2013MS000278.

Gottschalck, J., P. E. Roundy, C. J. Schreck III, A. Vintzileos, and C. Zhang (2013), Large-scale atmospheric and oceanic conditions during the 2011–12 DYNAMO field campaign, *Mon. Weather Rev.*, *141*, 4173–4196.

Haertel, P., K. Straub, and A. Budsock (2014), Transforming circumnavigating Kelvin waves that initiate and dissipate the Madden–Julian Oscillation, *Q. J. R. Meteorol. Soc.*, *141*, 1586–1602, doi:10.1002/qj.2461.

Heckley, W. A., and A. E. Gill (1984), Some simple analytical solutions to the problem of forced equatorial long waves, *Q. J. R. Meteorol. Soc.*, *110*, 203–217.

Hendon, H. H., and M. L. Salby (1994), The life cycle of the Madden–Julian Oscillation, *J. Atmos. Sci.*, *51*, 2225–2237.

Hoskins, B. J., and G.-Y. Yang (2000), The equatorial response to higher-latitude forcing, *J. Atmos. Sci.*, *57*, 1197–1213.

Hsu, H.-H., B. J. Hoskins, and F.-F. Jin (1990), The 1985/86 intraseasonal oscillation and the role of the extratropics, *J. Atmos. Sci.*, *47*, 823–839.

Inness, P. M., J. M. Slingo, E. Guilyardi, and J. Cole (2003), Simulation of the Madden–Julian Oscillation in a coupled general circulation model. Part II: The role of the basic state, *J. Clim.*, *16*, 365–382.

Janiga, M. A., and C. Zhang (2015), MJO moisture budget during DYNAMO in a cloud-permitting model, *J. Atmos. Sci.*, submitted.

Johnson, R. H., and P. E. Ciesielski (2013), Structure and properties of Madden–Julian Oscillations deduced from DYNAMO sounding arrays, *J. Atmos. Sci.*, *70*, 3157–3179.

Johnson, R. H., P. E. Ciesielski, J. H. Ruppert Jr., and M. Katsumata (2015), Sounding-based thermodynamic budgets for DYNAMO, *J. Atmos. Sci.*, *72*, 598–622.

Kerns, B. W., and S. S. Chen (2014), Equatorial dry air intrusion and related synoptic variability in MJO Initiation during DYNAMO, *Mon. Weather Rev.*, *142*, 1326–1343.

Kikuchi, K., and Y. N. Takayabu (2003), Equatorial circumnavigation of moisture signal associated with the Madden–Julian Oscillation (MJO) during boreal winter, *J. Meteorol. Soc. Jpn.*, *81*, 851–869.

Kim, D., J.-S. Kug, and A. H. Sobel (2014), Propagating versus nonpropagating Madden–Julian Oscillation events, *J. Clim.*, *27*, 111–125.

Kiranmayi, L., and E. D. Maloney (2011a), The intraseasonal moist static energy budget in reanalysis data, *J. Geophys. Res.*, *116*, D21117, doi:10.1029/2011JD016031.

Kiranmayi, L., and E. D. Maloney (2011b), Understanding intraseasonal variability in an aquaplanet GCM, *J. Meteorol. Soc. Jpn.*, *89*, 195–210, doi:10.2151/jmsj.2011-302.

Knutson, T. R., and K. M. Weickmann (1987), 30–60 Day atmospheric oscillations: Composite life cycles of convection and circulation anomalies, *Mon. Weather Rev.*, *115*, 1407–1436.

Majda, A. J., and S. N. Stechmann (2009), The skeleton of tropical intraseasonal oscillations, *Proc. Natl. Acad. Sci. U. S. A.*, *106*, 8417–8422.

Maloney, E. D. (2009), The moist static energy budget of a composite tropical intraseasonal oscillation in a climate model, *J. Clim.*, *22*, 711–729.

Maloney, E. D., and D. L. Hartmann (1998), Frictional moisture convergence in a composite lifecycle of the Madden–Julian Oscillation, *J. Clim.*, *11*, 2387–2403.

Maloney, E. D., and A. H. Sobel (2004), Surface fluxes and ocean coupling in the tropical intraseasonal oscillation, *J. Clim.*, *17*, 4368–4386.

Maloney, E. D., and S.-P. Xie (2013), Sensitivity of MJO activity to the pattern of climate warming, *J. Adv. Model. Earth Syst.*, *5*, 32–47, doi:10.1029/2012MS000171.

Maloney, E. D., A. H. Sobel, and W. M. Hannah (2010), Intraseasonal variability in an aquaplanet general circulation model, *J. Adv. Model. Earth Syst.*, *2*, 5, doi:10.3894/JAMES.2010.2.5.

Matthews, A. J. (2008), Primary and successive events in the Madden–Julian Oscillation, *Q. J. R. Meteorol. Soc.*, *13*, 439–453.

Moorthi, S., and M. J. Suarez (1992), Relaxed Arakawa-Schubert: A parameterization of moist convection for general circulation models, *Mon. Weather Rev.*, *120*, 978–1002.

Nasuno, T., T. Li, and K. Kikuchi (2015), Moistening processes before the convective initiation of Madden–Julian Oscillation events during the CINDY2011/DYNAMO period, *Mon. Weather Rev.*, *143*, 622–643.

Pan, L., and T. Li (2008), Interactions between the tropical ISO and mid-latitude low-frequency flow, *Clim. Dyn.*, *31*, 375–388, doi:10.1007/s00382-007-0272-7.

Peatman, S. C., A. J. Matthews, and D. P. Stevens (2014), Propagation of the Madden–Julian Oscillation through the Maritime Continent and scale interaction with the diurnal cycle of precipitation, *Q. J. R. Meteorol. Soc.*, *140*(680), 814–825.

Powell, S. W., and R. A. Houze (2013), The cloud population and onset of the Madden–Julian Oscillation over the Indian Ocean during DYNAMO-AMIE, *J. Geophys. Res.*, *118*, 11,979–11,995, doi:10.1002/2013JD020421.

Powell, S. W., and R. A. Houze Jr. (2015), Effect of dry large-scale vertical motions on initial MJO convective onset, *J. Geophys. Res. Atmos.*, *120*, 4783–4805, doi:10.1002/2014JD022961.
Pritchard, M. S., and C. S. Bretherton (2014), Causal evidence that rotational moisture advection is critical to the superparameterized Madden–Julian Oscillation, *J. Atmos. Sci.*, *71*, 800–815.
Ray, P., and T. Li (2013), Relative roles of circumnavigating waves and extratropics on the MJO and its relationship with the mean state, *J. Atmos. Sci.*, *70*, 876–893.
Ray, P., and C. Zhang (2010), A case study of the mechanics of extratropical influence on the initiation of the Madden–Julian Oscillation, *J. Atmos. Sci.*, *67*, 515–528.
Ray, P., C. Zhang, J. Dudhia, and S. S. Chen (2009), A numerical case study on the initiation of the Madden–Julian Oscillation, *J. Atmos. Sci.*, *66*, 310–331.
Ray, P., C. Zhang, M. W. Moncrieff, J. Dudhia, J. M. Caron, L. R. Leung, and C. Bruyere (2012), Role of the atmospheric mean state on the initiation of the Madden–Julian Oscillation in a tropical channel model, *Clim. Dyn.*, *36*, 161–184.
Raymond, D. J. (2001), A new model of the Madden–Julian Oscillation, *J. Atmos. Sci.*, *58*, 2807–2819.
Raymond, D. J., and Ž. Fuchs (2009), Moisture modes and the Madden–Julian Oscillation, *J. Clim.*, *22*, 3031–3046.
Roundy, P. E. (2014), Some aspects of Western Hemisphere Circulation and the Madden–Julian Oscillation, *J. Atmos. Sci.*, *71*, 2027–2039.
Ruppert, J. H., and R. H. Johnson (2015), Diurnally modulated cumulus moistening in the pre-onset stage of the Madden–Julian Oscillation during DYNAMO, *J. Atmos. Sci.*, *72*, 1622–1647.
Rydbeck, A. V., E. D. Maloney, S.-P. Xie, J. Hafner, and J. Shaman (2013), Remote forcing versus local feedback of east Pacific intraseasonal variability, *J. Clim.*, *26*, 3575–3596.
Shell, K. M., and I. M. Held (2004), Abrupt transition to strong superrotation in an axisymmetric model of the upper troposphere, *J. Atmos. Sci.*, *61*, 2928–2935.
Sobel, A. H., and E. D. Maloney (2012), An idealized semi-empirical framework for modeling the Madden–Julian Oscillation, *J. Atmos. Sci.*, *69*, 1691–1705.
Sobel, A. H., and E. D. Maloney (2013), Moisture modes and the eastward propagation of the MJO, *J. Atmos. Sci.*, *70*, 187–192.
Sobel, A. H., E. D. Maloney, G. Bellon, and D. M. Frierson (2010), Surface fluxes and tropical intraseasonal variability: A reassessment, *J. Adv. Model. Earth Syst.*, *2*, 2, doi:10.3894/JAMES.2010.2.2.
Sobel, A. H., S. Wang, and D. Kim (2014), Moist static energy budget of the MJO during DYNAMO, *J. Atmos. Sci.*, *71*, 4276–4291.
Straub, K. H. (2013), MJO initiation in the real-time multivariate MJO index, *J. Clim.*, *26*, 1130–1151.
Tokioka, T., K. Yamazaki, A. Kitoh, and T. Ose (1988), The equatorial 30–60 day oscillation and the Arakawa–Schubert penetrative cumulus parameterization, *J. Meteorol. Soc. Jpn.*, *66*, 883–901.
Wang, B., and X. Xie (1997), A model for the boreal summer intraseasonal oscillation, *J. Atmos. Sci.*, *54*, 72–86.
Wang, L., K. Kodera, and W. Chen (2012), Observed triggering of tropical convection by a cold surge: Implications for MJO initiation, *Q. J. R. Meteorol. Soc.*, *138*, 1740–1750.
Wang, S., A. H. Sobel, F. Zhang, Y. Q. Sun, Y. Yue, and L. Zhou (2015), Regional simulation of the October and November MJO events observed during the CINDY/DYNAMO field campaign at gray zone resolution, *J. Clim.*, *28*, 2097–2119.
Watanabe, M., and M. Kimoto (2000), Atmosphere-ocean thermal coupling in the North Atlantic: A positive feedback, *Q. J. R. Meteorol. Soc.*, *126*, 3343–3369.
Watanabe, M., and M. Kimoto (2001), Corrigendum, *Q. J. R. Meteorol. Soc.*, *127*, 733–734.
Webber, B. G. M., A. J. Matthews, and K. J. Heywood (2010), A dynamical ocean feedback mechanism for the Madden–Julian Oscillation, *Q. J. R. Meteorol. Soc.*, *136*, 740–754, doi:10.1002/qj.604.
Webber, B. G. M., A. J. Matthews, K. J. Heywood, and D. P. Stevens (2012), Ocean Rossby waves as a triggering mechanism for primary Madden–Julian events, *Q. J. R. Meteorol. Soc.*, *138*, 514–527.
Wheeler, M. C., and H. H. Hendon (2004), An all-season real-time multivariate MJO index: Development of an index for monitoring and prediction, *Mon. Weather Rev.*, *132*, 1917–1932.
Wolding, B. O. (2013), Moist static energy and the Madden–Julian Oscillation: Understanding initiation, maintenance, and propagation through the application of novel diagnostics, MS thesis, 132 pp., Colorado State Univ., Fort Collins, Colo.
Wolding, B. O., and E. D. Maloney (2015), Objective diagnostics and the Madden–Julian Oscillation. Part II: Application to moist static energy and moisture budgets, *J. Clim.*, doi:10.1175/JCLI-D-14-00689.1, in press.
Xu, W., and S. A. Rutledge (2014), Convective characteristics of the Madden–Julian Oscillation over the Central Indian Ocean Observed by Shipborne Radar during DYNAMO, *J. Atmos. Sci.*, *71*, 2859–2877.
Yoneyama, K., C. Zhang, and C. N. Long (2013), Tracking pulses of the Madden–Julian Oscillation, *Bull. Am. Meteorol. Soc.*, *94*, 1871–1891.
Zhang, G. J., and N. A. McFarlane (1995), Sensitivity of climate simulations to the parameterization of cumulus convection in the Canadian Climate Centre General Circulation Model, *Atmos. Ocean*, *33*, 407–446.
Zhao, C., T. Li, and T. Zhou (2013), Precursor signals and processes associated with MJO Initiation over the Tropical Indian Ocean, *J. Clim.*, *26*, 291–307.